

Constraints on Ultraheavy Dark Matter Properties from Dwarf Spheroidal Galaxies with LHAASO Observations

Zhen Cao,^{1,2,3} F. Aharonian,^{4,5} Q. An,^{6,7} Axikegu,⁸ Y. X. Bai,^{1,3} Y. W. Bao,⁹ D. Bastieri,¹⁰ X. J. Bi,^{1,2,3} Y. J. Bi,^{1,3,‡} J. T. Cai,¹⁰ Q. Cao,¹¹ W. Y. Cao,⁷ Zhe Cao,^{6,7} J. Chang,¹² J. F. Chang,^{1,3,6} A. M. Chen,¹³ E. S. Chen,^{1,2,3} Liang Chen,¹⁴ Lin Chen,⁸ Long Chen,⁸ M. J. Chen,^{1,3} M. L. Chen,^{1,3,6} Q. H. Chen,⁸ S. H. Chen,^{1,2,3} S. Z. Chen,^{1,3} T. L. Chen,¹⁵ Y. Chen,⁹ N. Cheng,^{1,3} Y. D. Cheng,^{1,3} M. Y. Cui,¹² S. W. Cui,¹¹ X. H. Cui,¹⁶ Y. D. Cui,¹⁷ B. Z. Dai,¹⁸ H. L. Dai,^{1,3,6} Z. G. Dai,⁷ Danzengluobu,¹⁵ D. della Volpe,¹⁹ X. Q. Dong,^{1,2,3} K. K. Duan,¹² J. H. Fan,¹⁰ Y. Z. Fan,¹² J. Fang,¹⁸ K. Fang,^{1,3} C. F. Feng,²⁰ L. Feng,¹² S. H. Feng,^{1,3} X. T. Feng,²⁰ Y. L. Feng,¹⁵ S. Gabici,²¹ B. Gao,^{1,3} C. D. Gao,²⁰ L. Q. Gao,^{1,2,3,§} Q. Gao,¹⁵ W. Gao,^{1,3} W. K. Gao,^{1,2,3} M. M. Ge,¹⁸ L. S. Geng,^{1,3} G. Giacinti,¹³ G. H. Gong,²² Q. B. Gou,^{1,3} M. H. Gu,^{1,3,6} F. L. Guo,¹⁴ X. L. Guo,⁸ Y. Q. Guo,^{1,3} Y. Y. Guo,¹² Y. A. Han,²³ H. H. He,^{1,2,3} H. N. He,¹² J. Y. He,¹² X. B. He,¹⁷ Y. He,⁸ M. Heller,¹⁹ Y. K. Hor,¹⁷ B. W. Hou,^{1,2,3} C. Hou,^{1,3} X. Hou,²⁴ H. B. Hu,^{1,2,3} Q. Hu,^{7,12} S. C. Hu,^{1,2,3} D. H. Huang,⁸ T. Q. Huang,^{1,3} W. J. Huang,¹⁷ X. T. Huang,²⁰ X. Y. Huang,^{12,||} Y. Huang,^{1,2,3} Z. C. Huang,⁸ X. L. Ji,^{1,3,6} H. Y. Jia,⁸ K. Jia,^{20,*} K. Jiang,^{6,7} X. W. Jiang,^{1,3} Z. J. Jiang,¹⁸ M. Jin,⁸ M. M. Kang,²⁵ T. Ke,^{1,3} D. Kuleshov,²⁶ K. Kurinov,^{26,27} B. B. Li,¹¹ Cheng Li,^{6,7} Cong Li,^{1,3} D. Li,^{1,2,3} F. Li,^{1,3,6} H. B. Li,^{1,3} H. C. Li,^{1,3} H. Y. Li,^{7,12} J. Li,^{7,12,†} Jian Li,⁷ Jie Li,^{1,3,6} K. Li,^{1,3} W. L. Li,^{20,¶} W. L. Li,¹³ X. R. Li,^{1,3} Xin Li,^{6,7} Y. Z. Li,^{1,2,3} Zhe Li,^{1,3} Zhuo Li,²⁸ E. W. Liang,²⁹ Y. F. Liang,²⁹ S. J. Lin,¹⁷ B. Liu,⁷ C. Liu,^{1,3} D. Liu,²⁰ H. Liu,⁸ H. D. Liu,²³ J. Liu,^{1,3} J. L. Liu,^{1,3} J. Y. Liu,^{1,3} M. Y. Liu,¹⁵ R. Y. Liu,⁹ S. M. Liu,⁸ W. Liu,^{1,3} Y. Liu,¹⁰ Y. N. Liu,²² R. Lu,¹⁸ Q. Luo,¹⁷ H. K. Lv,^{1,3} B. Q. Ma,²⁸ L. L. Ma,^{1,3} X. H. Ma,^{1,3} J. R. Mao,²⁴ Z. Min,^{1,3} W. Mitthumsiri,³⁰ H. J. Mu,²³ Y. C. Nan,^{1,3} A. Neronov,²¹ Z. W. Ou,¹⁷ B. Y. Pang,⁸ P. Pattarakijwanich,³⁰ Z. Y. Pei,¹⁰ M. Y. Qi,^{1,3} Y. Q. Qi,¹¹ B. Q. Qiao,^{1,3} J. J. Qin,⁷ D. Ruffolo,³⁰ A. Sáiz,³⁰ D. Semikoz,²¹ C. Y. Shao,¹⁷ L. Shao,¹¹ O. Shchegolev,^{26,27} X. D. Sheng,^{1,3} F. W. Shu,³¹ H. C. Song,²⁸ Yu. V. Stenkin,^{26,27} V. Stepanov,²⁶ Y. Su,¹² Q. N. Sun,⁸ X. N. Sun,²⁹ Z. B. Sun,³² P. H. T. Tam,¹⁷ Q. W. Tang,³¹ Z. B. Tang,^{6,7} W. W. Tian,^{2,16} C. Wang,³² C. B. Wang,⁸ G. W. Wang,⁷ H. G. Wang,¹⁰ H. H. Wang,¹⁷ J. C. Wang,²⁴ K. Wang,⁹ L. P. Wang,²⁰ L. Y. Wang,^{1,3} P. H. Wang,⁸ R. Wang,²⁰ W. Wang,¹⁷ X. G. Wang,²⁹ X. Y. Wang,⁹ Y. Wang,⁸ Y. D. Wang,^{1,3} Y. J. Wang,^{1,3} Z. H. Wang,²⁵ Z. X. Wang,¹⁸ Zhen Wang,¹³ Zheng Wang,^{1,3,6} D. M. Wei,¹² J. J. Wei,¹² Y. J. Wei,^{1,2,3} T. Wen,¹⁸ C. Y. Wu,^{1,3} H. R. Wu,^{1,3} S. Wu,^{1,3} X. F. Wu,¹² Y. S. Wu,⁷ S. Q. Xi,^{1,3} J. Xia,^{7,12} J. J. Xia,⁸ G. M. Xiang,^{2,14} D. X. Xiao,¹¹ G. Xiao,^{1,3} G. G. Xin,^{1,3} Y. L. Xin,⁸ Y. Xing,¹⁴ Z. Xiong,^{1,2,3} D. L. Xu,¹³ R. F. Xu,^{1,2,3} R. X. Xu,²⁸ W. L. Xu,²⁵ L. Xue,²⁰ D. H. Yan,¹⁸ J. Z. Yan,¹² T. Yan,^{1,3} C. W. Yang,²⁵ F. Yang,¹¹ F. F. Yang,^{1,3,6} H. W. Yang,¹⁷ J. Y. Yang,¹⁷ L. L. Yang,¹⁷ M. J. Yang,^{1,3} R. Z. Yang,⁷ S. B. Yang,¹⁸ Y. H. Yao,²⁵ Z. G. Yao,^{1,3} Y. M. Ye,²² L. Q. Yin,^{1,3} N. Yin,²⁰ X. H. You,^{1,3} Z. Y. You,^{1,2,3} Y. H. Yu,⁷ Q. Yuan,¹² H. Yue,^{1,2,3} H. D. Zeng,¹² T. X. Zeng,^{1,3,6} W. Zeng,¹⁸ M. Zha,^{1,3} B. B. Zhang,⁹ F. Zhang,⁸ H. M. Zhang,⁹ H. Y. Zhang,^{1,3} J. L. Zhang,¹⁶ L. X. Zhang,¹⁰ Li Zhang,¹⁸ P. F. Zhang,¹⁸ P. P. Zhang,^{7,12} R. Zhang,^{7,12} S. B. Zhang,^{2,16} S. R. Zhang,¹¹ S. S. Zhang,^{1,3} X. Zhang,⁹ X. P. Zhang,^{1,3} Y. F. Zhang,⁸ Yi Zhang,^{1,12} Yong Zhang,^{1,3} B. Zhao,⁸ J. Zhao,^{1,3} L. Zhao,^{6,7} L. Z. Zhao,¹¹ S. P. Zhao,^{12,20} F. Zheng,³² B. Zhou,^{1,3} H. Zhou,¹³ J. N. Zhou,¹⁴ M. Zhou,³¹ P. Zhou,⁹ R. Zhou,²⁵ X. X. Zhou,⁸ C. G. Zhu,^{20,**} F. R. Zhu,⁸ H. Zhu,¹⁶ K. J. Zhu,^{1,2,3,6} and X. Zuo^{1,3}

(LHAASO Collaboration)

¹Key Laboratory of Particle Astrophysics and Experimental Physics Division and Computing Center, Institute of High Energy Physics, Chinese Academy of Sciences, 100049 Beijing, China

²University of Chinese Academy of Sciences, 100049 Beijing, China

³Tianfu Cosmic Ray Research Center, 610000 Chengdu, Sichuan, China

⁴Dublin Institute for Advanced Studies, 31 Fitzwilliam Place, 2 Dublin, Ireland

⁵Max-Planck-Institut für Nuclear Physics, P.O. Box 103980, 69029 Heidelberg, Germany

⁶State Key Laboratory of Particle Detection and Electronics, China

⁷University of Science and Technology of China, 230026 Hefei, Anhui, China

⁸School of Physical Science and Technology and School of Information Science and Technology, Southwest Jiaotong University, 610031 Chengdu, Sichuan, China

⁹School of Astronomy and Space Science, Nanjing University, 210023 Nanjing, Jiangsu, China


¹⁰Center for Astrophysics, Guangzhou University, 510006 Guangzhou, Guangdong, China

¹¹Hebei Normal University, 050024 Shijiazhuang, Hebei, China

¹²Key Laboratory of Dark Matter and Space Astronomy and Key Laboratory of Radio Astronomy, Purple Mountain Observatory, Chinese Academy of Sciences, 210023 Nanjing, Jiangsu, China

¹³Tsung-Dao Lee Institute and School of Physics and Astronomy, Shanghai Jiao Tong University, 200240 Shanghai, China

- ¹⁴Key Laboratory for Research in Galaxies and Cosmology, Shanghai Astronomical Observatory, Chinese Academy of Sciences, 200030 Shanghai, China
- ¹⁵Key Laboratory of Cosmic Rays (Tibet University), Ministry of Education, 850000 Lhasa, Tibet, China
- ¹⁶National Astronomical Observatories, Chinese Academy of Sciences, 100101 Beijing, China
- ¹⁷School of Physics and Astronomy (Zhuhai) and School of Physics (Guangzhou) and Sino-French Institute of Nuclear Engineering and Technology (Zhuhai), Sun Yat-sen University, 519000 Zhuhai and 510275 Guangzhou, Guangdong, China
- ¹⁸School of Physics and Astronomy, Yunnan University, 650091 Kunming, Yunnan, China
- ¹⁹Département de Physique Nucléaire et Corpusculaire, Faculté de Sciences, Université de Genève, 24 Quai Ernest Ansermet, 1211 Geneva, Switzerland
- ²⁰Institute of Frontier and Interdisciplinary Science, Shandong University, 266237 Qingdao, Shandong, China
- ²¹APC, Université Paris Cité, CNRS/IN2P3, CEA/IRFU, Observatoire de Paris, 119 75205 Paris, France
- ²²Department of Engineering Physics, Tsinghua University, 100084 Beijing, China
- ²³School of Physics and Microelectronics, Zhengzhou University, 450001 Zhengzhou, Henan, China
- ²⁴Yunnan Observatories, Chinese Academy of Sciences, 650216 Kunming, Yunnan, China
- ²⁵College of Physics, Sichuan University, 610065 Chengdu, Sichuan, China
- ²⁶Institute for Nuclear Research of Russian Academy of Sciences, 117312 Moscow, Russia
- ²⁷Moscow Institute of Physics and Technology, 141700 Moscow, Russia
- ²⁸School of Physics, Peking University, 100871 Beijing, China
- ²⁹School of Physical Science and Technology, Guangxi University, 530004 Nanning, Guangxi, China
- ³⁰Department of Physics, Faculty of Science, Mahidol University, 10400 Bangkok, Thailand
- ³¹Center for Relativistic Astrophysics and High Energy Physics, School of Physics and Materials Science and Institute of Space Science and Technology, Nanchang University, 330031 Nanchang, Jiangxi, China
- ³²National Space Science Center, Chinese Academy of Sciences, 100190 Beijing, China

 (Received 31 October 2023; revised 1 May 2024; accepted 12 June 2024; published 6 August 2024)

In this Letter we try to search for signals generated by ultraheavy dark matter at the Large High Altitude Air Shower Observatory (LHAASO) data. We look for possible γ rays by dark matter annihilation or decay from 16 dwarf spheroidal galaxies in the field of view of the LHAASO. Dwarf spheroidal galaxies are among the most promising targets for indirect detection of dark matter that have low fluxes of astrophysical γ -ray background while having large amount of dark matter. By analyzing more than 700 days of observational data at LHAASO, no significant dark matter signal from 1 TeV to 1 EeV is detected. Accordingly we derive the most stringent constraints on the ultraheavy dark matter annihilation cross section up to EeV. The constraints on the lifetime of dark matter in decay mode are also derived.

DOI: [10.1103/PhysRevLett.133.061001](https://doi.org/10.1103/PhysRevLett.133.061001)

Introduction—Various kinds of astronomical evidence suggest the existence of massive dark matter (DM) in the Universe [1], which comprises approximately 85% of all matter [2]. However, DM cannot be explained by the standard model of particle physics [3,4]. Therefore, one of the most important tasks in fundamental physics is to detect and reveal the nature of DM particles. Most searches primarily focus on weakly interacting massive particles or ultralight DM. However, no conclusive DM signal has been observed up to now [5–9]. On the other hand, ultraheavy dark matter (UHDM; $10 \lesssim M_\chi \lesssim m_{pl} \approx 10^{16}$ TeV) represents a potential alternative DM candidate that could be generated through various mechanisms, including freeze-out,

freeze-in, out-of-equilibrium decay, phase transitions, gravitational particle production, and primordial black holes (see the review in Ref. [10] and references therein). Some models for UHDM, like composite dark matter [11–13], have been proposed to evade the unitarity limit, and very-high-energy (VHE) γ -rays may be produced not only via the decay of UHDM, but also via its self-annihilation [14].

Among different astronomical systems, dwarf spheroidal galaxies (dSphs) are considered one of the most promising targets for detecting DM signals due to their relatively short distances, high mass-to-light ratios [15,16], and locations far away from complicated emission regions like the Galactic disk. These properties have instigated extensive research on them utilizing various astronomical facilities [17–26]. Importantly, given the relative proximity of these systems, the angular dimensions of their signal regions, particularly in scenarios involving decay, may be comparable to or even surpass the point spread function (PSF) of detection instruments. Thus, viewing these sources as extended rather than pointlike sources may play a crucial role in the indirect detection of DM [27,28].

* Contact author: jjakang@mail.sdu.edu.cn

† Contact author: lij@pmo.ac.cn

‡ Contact author: bixj@ihep.ac.cn

§ Contact author: gaolinqing@hotmail.com

|| Contact author: xyhuang@pmo.ac.cn

¶ Contact author: liwl@mail.sdu.edu.cn

** Contact author: zhucg@email.sdu.edu.cn

The Large High Altitude Air Shower Observatory (LHAASO) is located in Sichuan Province, China, at an altitude of 4410 m. It is a multipurpose and comprehensive extensive air shower array, designed for the study of cosmic rays and γ rays across wide energy ranges, from 10 TeV to 100 PeV for cosmic rays and from sub-TeV to beyond 1 PeV for γ rays [29]. LHAASO is composed of three subarrays: the kilometer-square array (KM2A), the water Cherenkov detector array (WCDA), and the wide field-of-view air Cherenkov telescope array. Since its operation, several important results have been achieved in cosmic- and γ -ray research [30–34]. The remarkable γ -ray sensitivity of LHAASO for energies exceeding 100 TeV [35] presents an opportunity for the exploration of UHDM. WCDA and KM2A also have good PSFs for VHE γ rays [36,37], enabling them to potentially discern the spatial extension of dSphs.

In this Letter, we search for VHE γ -ray signal from dSphs with data recorded by WCDA and KM2A of LHAASO and report the stringent constraints on the UHDM up to EeV.

γ -ray flux from dark matter—The expected differential γ -ray flux from DM annihilation can be written as

$$\frac{dF_{\text{anni}}}{dEd\Omega dt}(E, \Omega) = \frac{\langle \sigma_A v \rangle}{8\pi M_\chi^2} \frac{dN_\gamma}{dE} e^{-\tau_{rr}(E)} \times \frac{dJ}{d\Omega}. \quad (1)$$

Similarly, for DM decay, it can be defined as

$$\frac{dF_{\text{decay}}}{dEd\Omega dt}(E, \Omega) = \frac{1}{4\pi\tau_\chi M_\chi} \frac{dN_\gamma}{dE} e^{-\tau_{rr}(E)} \times \frac{dD}{d\Omega}, \quad (2)$$

where $\langle \sigma_A v \rangle$ is the velocity-weighted DM annihilation cross section, τ_χ is the DM decay lifetime, and M_χ is the mass of the DM particle. dN_γ/dE is the γ -ray energy spectrum resulting from DM annihilation (decay), as calculated using HDMSpectra [38]. The term $\tau_{rr}(E)$ represents the total attenuation depth resulting from the pair production process ($\gamma\gamma \rightarrow e^+e^-$), taking into account background photons from starlight, infrared radiation, and cosmic microwave background, as described in Ref. [39]. The last term is the differential $J(D)$ factor, which characterizes the strength of the DM signal. In Eqs. (1) and (2), $dJ/d\Omega = \int \rho_{\text{DM}}^2(r) dl$ and $dD/d\Omega = \int \rho_{\text{DM}}(r) dl$, where $\rho_{\text{DM}}(r)$ refers to the DM density at distance r from the center of dSphs, and l represents the distance from a point on the line of sight to Earth. The $J(D)$ factor is defined as the differential $J(D)$ factor integrated over the region of interest (ROI). In this Letter, we take the DM density distribution in dSphs following the Navarro-Frenk-White (NFW) profile [40].

With a large field of view (FOV) of approximately 2 sr, LHAASO has the ability to observe about 60% of the sky each day [35]. The 16 dSphs within the FOV of LHAASO have been selected as our observation targets, and the coordinates of these dSphs are shown in Table I of the Supplemental Material [41]. To optimize the size of the ROI for balancing the preference between a larger area containing more signal and a smaller area with less background (and nearby sources) contamination, we utilize

S/\sqrt{B} as a metric, where S and B are the expected signal and expected background in the ROI, respectively. Considering the expected signal also depends on the details of the NFW profile [46–48], we use the publicly available Markov chain Monte Carlo chains provided by Ref. [48] to determine the optimal ROI for our instrument and compute the corresponding $J(D)$ factor distribution in our ROI. The details are discussed in Sec. II of the Supplemental Material. The half-width of the chosen ROI, the corresponding median $J(D)$ factor, and its uncertainty for each dSph are shown in Table I. For the observation of WCDA, it is a conservative case that the ROI selection is consistent with the above value because WCDA has better angular resolution in the low-energy range than KM2A. Meanwhile, the $J(D)$ factor is consistent throughout the analysis.

Observation and data analysis—The present Letter utilizes LHAASO-WCDA data ($E < 20$ TeV) acquired from March 5, 2021 to March 31, 2023. LHAASO-KM2A data ($E > 10$ TeV) are utilized, including KM2A 1/2 array data from December 27, 2019 to November 30, 2020, KM2A 3/4 array data from December 1, 2020 to July 19, 2021, and KM2A full array data from July 20, 2021 to February 28, 2022. We apply the detector simulation, event reconstruction, and selection algorithms detailed in the performance papers of LHAASO subarrays [36,37] for the analysis of WCDA and KM2A data. The total effective observation time for each target dSph from WCDA and KM2A are shown in Table I of Supplemental Material [41].

We divide the KM2A data from 10 to 10^3 TeV into ten logarithmically evenly spaced bins according to reconstructed energy. For the WCDA data, events are divided into six groups according to the number of triggered photomultiplier tube units (N_{hits}), i.e., [60,100], [100,200], [200,300], [300,500], [500,800], [800,2000]. Based on the reconstructed direction, the selected events from each energy bin in the KM2A dataset and each group of WCDA data are mapped onto a 2D sky map with a pixel size of $0.1^\circ \times 0.1^\circ$ in the equatorial coordinate. We use the “direct integration” method as described in Ref. [49] to estimate the number of background events per pixel. To eliminate the contamination of known γ -ray sources on background estimation, we mask the Galactic disk region ($|b| < 10^\circ$), known sources given by TeVCat [50] and first LHAASO catalog [51] (see Fig. 1 of Supplemental Material [41]).

The expected numbers of γ -ray events produced by DM in the regions of interest are calculated by folding the γ -ray flux produced by DM with the WCDA and KM2A detector response function respectively. More details are discussed in Sec. I of Supplemental Material [41].

To quantify the excess of γ -ray signals in the regions of interest, we use a 3D binned likelihood ratio analysis combining WCDA and KM2A data. This method accounts for both the energy spectrum and the spatial characteristics of the DM signals, which are different from the background

TABLE I. The ROI half-width and J (D) factor for 16 dSphs considered in this analysis.

Name	$\log_{10}(J_\theta/\text{GeV}^2 \text{cm}^{-5})$	θ_{anni} (deg)	$\log_{10}(D_\theta/\text{GeV cm}^{-2})$	θ_{decay} (deg)
Draco	$18.96^{+0.16}_{-0.15}$	1.0	$19.38^{+0.24}_{-0.32}$	2.3
Ursa Minor	$18.79^{+0.12}_{-0.11}$	1.0	$18.68^{+0.33}_{-0.15}$	2.1
Ursa Major I	$18.40^{+0.28}_{-0.27}$	0.9	$18.64^{+0.50}_{-0.48}$	1.8
Ursa Major II	$19.70^{+0.43}_{-0.43}$	1.0	$19.41^{+0.43}_{-0.57}$	2.0
Bootes 1	$18.39^{+0.36}_{-0.37}$	0.9	$18.77^{+0.40}_{-0.54}$	1.8
Canes Venatici I	$17.43^{+0.16}_{-0.15}$	0.8	$18.19^{+0.40}_{-0.39}$	1.3
Coma Berenices	$19.26^{+0.35}_{-0.43}$	0.9	$19.12^{+0.46}_{-0.73}$	1.8
Leo I	$17.58^{+0.10}_{-0.10}$	0.8	$18.44^{+0.33}_{-0.42}$	1.4
Segue 1	$19.25^{+0.60}_{-0.69}$	0.8	$18.33^{+0.69}_{-0.63}$	0.8
Sextans	$17.80^{+0.10}_{-0.10}$	1.0	$18.49^{+0.28}_{-0.21}$	1.8
Canes Venatici II	$17.82^{+0.38}_{-0.37}$	0.8	$18.45^{+0.50}_{-0.74}$	1.4
Hercules	$17.60^{+0.53}_{-0.69}$	0.8	$17.79^{+0.62}_{-0.61}$	1.0
Leo II	$17.72^{+0.18}_{-0.17}$	0.8	$17.85^{+0.62}_{-0.40}$	1.0
Willman I	$19.80^{+0.50}_{-0.52}$	0.9	$19.00^{+0.71}_{-0.93}$	1.5
Aquarius 2	$18.57^{+0.50}_{-0.57}$	1.1	$18.53^{+0.61}_{-0.68}$	1.3
Leo T	$17.66^{+0.55}_{-0.52}$	0.8	$17.88^{+0.65}_{-0.69}$	1.0

in the regions of interest. In this analysis, we define the 3D likelihood function for the k th dSph as follows:

$$\mathcal{L}_k = \prod_{i,j} \text{Poisson}(N_{i,j,k}^{\text{obs}}; N_{i,j,k}^{\text{exp}} + N_{i,j,k}^{\text{bkg}}) \times \mathcal{G}(B_k; B_k^{\text{obs}}, \sigma_k), \quad (3)$$

where

$$\mathcal{G}(B_k; B_k^{\text{obs}}, \sigma_k) = \frac{1}{\ln(10) B_k^{\text{obs}} \sqrt{2\pi} \sigma_k} e^{-[\log_{10}(B_k) - \log_{10}(B_k^{\text{obs}})]^2 / 2\sigma_k^2}. \quad (4)$$

The $N_{i,j,k}^{\text{exp}}$ is the expected number of γ rays from DM annihilation or decay in the i th energy estimator bin and the j th pixel on the 2D sky map of the k th dSph. $N_{i,j,k}^{\text{bkg}}$ is the estimated background events from the direct integration method, and $N_{i,j,k}^{\text{obs}}$ is the observed number of γ -ray photons. The term $\mathcal{G}(B_k; B_k^{\text{obs}}, \sigma_k)$ is included for the statistical uncertainties on the J (D) factor of the k th dSph, following Refs. [17,18], where B equals J for the annihilation case and B equals D for the decaying case. The larger uncertainties listed in Table I are taken as σ_k considering the asymmetric distribution of the J (D) factor conservatively.

To quantify how well the DM signal fits the observed data, we define the test statistic of the k th dSph (TS_k) as

$$TS_k = -2 \ln \left(\frac{\mathcal{L}_k(S=0)}{\mathcal{L}_k(S_{\text{max}})} \right), \quad (5)$$

where S represents the DM signal flux, and S_{max} is the best-fit value of the DM signal flux that maximizes the likelihood. To avoid nonphysical values, we set $\langle \sigma_A v \rangle$ and τ_χ to be positive during the fitting process. We obtained the statistical significance of the signal over the null hypothesis (no DM model) by $\sqrt{TS_k}$. Then one-sided 95% confidence level (C.L.) limits on $\langle \sigma_A v \rangle$ or τ_χ are set by increasing the DM signal normalization from its best-fit value until $-2 \ln \mathcal{L}$ increases by a value of 2.71 [52].

The combined likelihood analysis of all dSphs is performed by $\mathcal{L}_{\text{total}} = \prod_k \mathcal{L}_k$, with the aim of improving the overall statistical power and generating stronger constraints on the DM parameters.

Results—We utilize data from 756 days of LHAASO-WCDA and 794 days of LHAASO-KM2A observations to search for DM signals in 16 dSphs around the Milky Way. No significant γ -ray excess was detected from these dSphs. The statistical significance of DM signals in these dSphs is shown in Sec. III of Supplemental Material [41]. Therefore, 95% C.L. limits are placed on the DM annihilation cross section or the DM decay lifetime, as shown in Figs. 1 and 2, respectively. In Fig. 8 of Supplemental Material [41], the 95% C.L. upper limits for $\langle \sigma_A v \rangle$ from combined and individual dSphs are presented, assuming a DM mass range from 1 TeV to 1 EeV with a 100% branching ratio to specific standard model particles. The combined upper limits are dominated by sources with large J factor, small uncertainties, and favorable locations inside the LHAASO FOV, i.e., Ursa Major II, Ursa Minor, Draco, Willman I, Segue 1, and Coma Berenices.

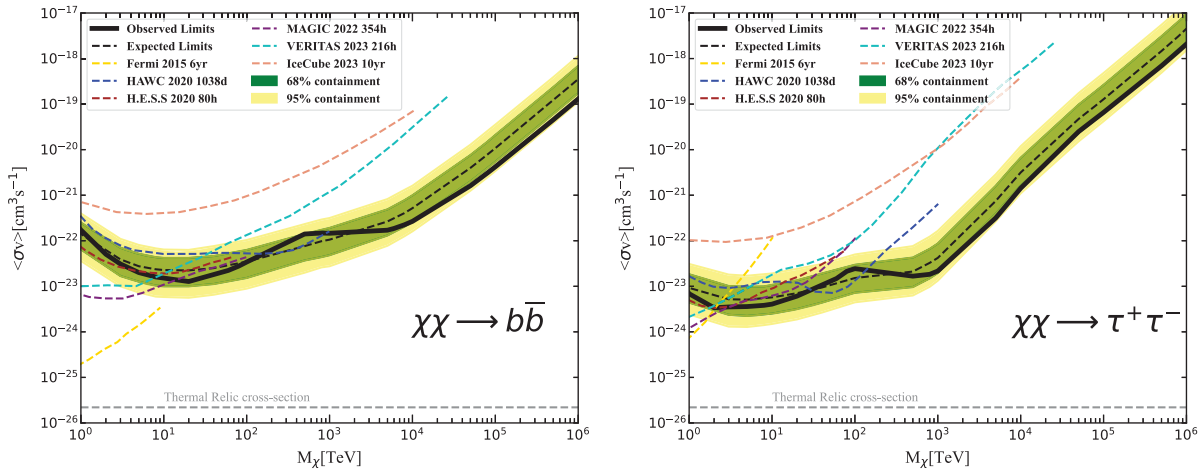


FIG. 1. The 95% C.L. upper limits on the DM annihilation cross section for $b\bar{b}$, $\tau^+\tau^-$ channels and comparing to other experiments (Fermi-LAT [18], HAWC [20], H.E.S.S. [21], MAGIC [22], VERITAS [23], IceCube [53]). The solid black line represents the observed combined limit of this Letter. The dashed black line, green band, and yellow band represent the expected limits and their 1σ and 2σ uncertainties. The dashed gray line is the thermal relic cross section [54], and the other dashed colored lines show the results of other experiments.

To assess the consistency between the constraints derived from the observed data and the expected limits from pure background, we repeat 1000 mock observations under the null hypothesis, considering the Poisson fluctuation with the measured background. The expected combined limits and the two-sided 68% and 95% containment bands for $b\bar{b}$ and $\tau^+\tau^-$ are shown in Fig. 1. See also Fig. 10 of the Supplemental Material [41] for other channels. The fact that observed limits are between the expected limit bands indicates that the observational data are consistent with Poisson fluctuation with the background. The constraints on high-mass DM consistently approach the 68% boundary of the anticipated limit bands, suggesting a slight

overestimation of the background in this study and thereby a deficit in the number of putative signal events inferred in the regions of interest. This overestimation is likely due to the contribution of faint sources which are below our sensitivity threshold and thus not removed by the mask used in our background estimation; this issue may be more important for high masses due to the lower event rates at high energies. Figure 1 also shows the “thermal relic” cross section [54] and the limits from other experiments such as Fermi-LAT [18], HAWC [20], H.E.S.S. [21], MAGIC [22], VERITAS [23], and IceCube [53]. The observations of dSphs by LHAASO could provide better constraints for DM with a mass heavier than a few hundred TeV.

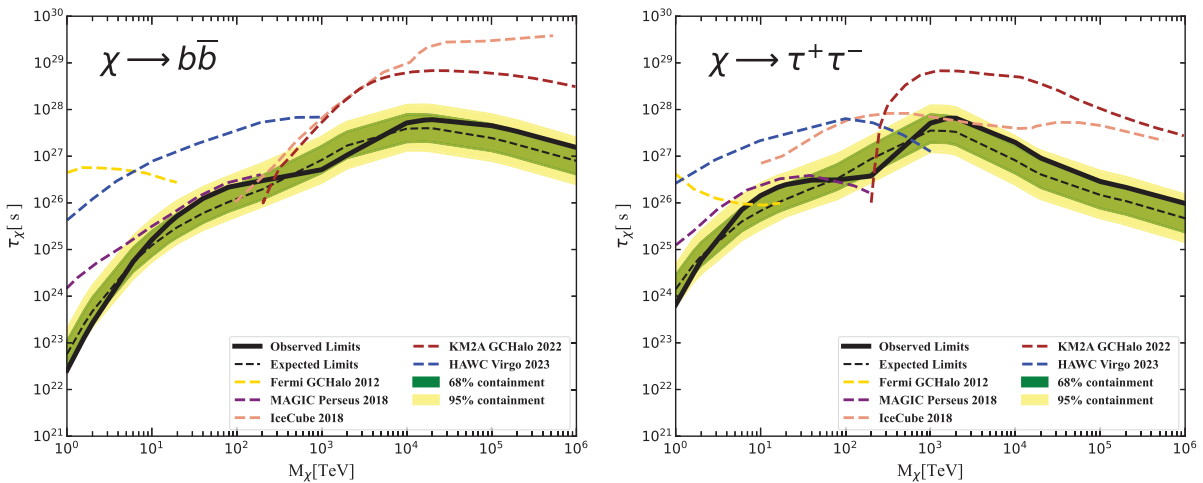


FIG. 2. The 95% C.L. lower limits on the DM decay lifetime for $b\bar{b}$, $\tau^+\tau^-$ channels. The solid black line represents the LHAASO observed combined limit, and the dashed black line, green band, and yellow band represent the expected combined limits, 1σ and 2σ uncertainty based on the mock observation. The limits obtained from Fermi-LAT [55], MAGIC [56], IceCube [57], LHAASO-KM2A Galactic halo [32], and HAWC [58] with dashed colored lines are also shown for comparison.

In Fig. 9 of Supplemental Material [41], the 95% C.L. lower limits for τ_χ are presented for combined and individual dSphs analysis. Similar to the DM annihilation results, the limits are mainly driven by Ursa Major II, Ursa Minor, Draco, and Coma Berenices. The expected limits from the same analysis for mock data are shown in Fig. 2, for $b\bar{b}$ and $\tau^+\tau^-$ final states, with the limits from Fermi-LAT [55], MAGIC [56], IceCube [57], LHAASO-KM2A Galactic halo [32], and HAWC [58]. We also show constraints for τ_χ from combined dSphs observation and mock data in Fig. 10 of Supplemental Material [41] for other channels.

In our analysis, we incorporate the $J(D)$ factor likelihood into our likelihood analysis, leading to a reduction in the constraints on DM parameters by a factor of 2–6 (see Fig. 6 of Supplemental Material [41]). Additionally, we factor in the effects of VHE γ -ray absorption by the interstellar radiation field, resulting in a relaxation of constraints on DM particles with masses exceeding 1000 TeV by approximately five- to tenfold. Moreover, we consider the expected morphology of the DM signal, moving beyond a pointlike source approximation. The constraints derived from the extended source analysis based on the DM density profile are consequently diminished by a factor of 1.5–12, particularly in the context of DM decay scenarios, conforming a strong effect of the spatial extension of dSphs on the DM search results [28]. It is important to acknowledge that the $J(D)$ factor correction exclusively accounts for the statistical uncertainties in the $J(D)$ factors and does not address the systematic uncertainties stemming from the choice of DM profiles and uncertainties with some presumptions about the Jeans equations. While factors such as departures from spherical symmetry, velocity anisotropy of the DM halo, the influence of contaminating foreground stars, and variations in the DM profile are considered, the predicted $J(D)$ factors and constraints may undergo alterations by a fewfold [18,59–65].

Our results extend for the first time the mass range of the limits on the $\langle\sigma_A v\rangle$ to 1 EeV with the best constraints above a few hundred TeV. Fermi-LAT [18], H.E.S.S. [21], MAGIC [22], and VERITAS [23] exhibit more stringent limits at lower DM masses, since the effective area of LHAASO would decay rapidly at low energy. We have comparable limits to HAWC [20] for masses up to several hundred TeV and consistently have better constraints than those from IceCube [53] across all mass ranges. For the DM decay lifetime, our constraints are weaker than those based on galactic halo data by KM2A [32], since the D factor in the selected dSphs is smaller, and the effects of attenuation by pair production are more significant considering the large distances of dSphs from Earth compared to the Galactic halo. In general, our constraints on the DM decay lifetime are also less stringent compared to those determined by HAWC [58], MAGIC [56], Fermi-LAT [55],

and IceCube [57] through the observation of Virgo cluster, Perseus cluster, and the Galactic halo with larger D factors and subdominant effects of attenuation. However, the combined limits from dSphs, considering the uncertainties of the DM distribution and the spatial extension of the expected signal, could also provide a complementary set of reliable limits.

Conclusion and outlook—We investigate DM annihilation and decay signals from 16 dSphs within the LHAASO FOV using data collected by WCDA and KM2A. No significant γ -ray excess is observed from these sources. Consequently, we establish individual and combined constraints on $\langle\sigma_A v\rangle$ and τ_χ across five channels ($b\bar{b}, t\bar{t}, \mu^+\mu^-, \tau^+\tau^-, W^+W^-$).

In this analysis, we treat the selected dSphs as extended sources in the 3D likelihood analysis framework to consider the spatial distribution of the DM density within the dSphs. We optimize the size of regions of interest and recalculate the $J(D)$ factor and their uncertainties corresponding to the regions of interest. To make the analysis more comprehensive and reliable, the absorption effect of ISRF on VHE γ ray is considered, and the statistical uncertainty of the $J(D)$ factor is incorporated as a nuisance parameter in the likelihood analysis.

Our results represent the first-ever constraint on $\langle\sigma_A v\rangle$, extending the mass of DM to 1 EeV. The combined limits are the most stringent constraints for $\langle\sigma_A v\rangle$ above a few hundred TeV. Meanwhile, we stress that the impact of spatial extension from dSphs is a necessary condition when deriving DM limits from dSphs with future instruments. As more WCDA and KM2A data will be collected, the development of algorithms to enhance energy and angular resolution for LHAASO, and improvements in kinematics measurements to reduce the uncertainty of the DM density distribution, LHAASO is expected to become more sensitive and to improve its limits in the future.

Acknowledgments—We would like to thank all staff members who work at the LHAASO site above 4400 meters above sea level year-round to maintain the detector and keep the water recycling system, electricity power supply and other components of the experiment operating smoothly. We are grateful to Chengdu Management Committee of Tianfu New Area for the constant financial support for research with LHAASO data. This research work is supported by the following grants: The National Key R&D program of China No. 2018YFA0404201, No. 2018YFA0404202, No. 2018YFA0404203, No. 2018YFA0404204, National Natural Science Foundation of China No. 12175248, No. 12322302, Department of Science and Technology of Sichuan Province, China No. 2021YFSY0030, Project for Young Scientists in Basic Research of Chinese Academy of Sciences No. YSBR-061, the Chinese Academy of Sciences, the Program for Innovative Talents and

Entrepreneur in Jiangsu, and in Thailand by the National Science and Technology Development Agency (NSTDA) and the National Research Council of Thailand (NRCT) under the High-Potential Research Team Grant Program (N42A650868).

-
- [1] G. Bertone, D. Hooper, and J. Silk, Particle dark matter: Evidence, candidates and constraints, *Phys. Rep.* **405**, 279 (2005).
- [2] N. Aghanim *et al.* (Planck Collaboration), Planck 2018 results. VI. Cosmological parameters, *Astron. Astrophys.* **641**, A6 (2020); **652**, C4(E) (2021).
- [3] G. Jungman, M. Kamionkowski, and K. Griest, Supersymmetric dark matter, *Phys. Rep.* **267**, 195 (1996).
- [4] L. Bergström, Dark matter evidence, particle physics candidates and detection methods, *Ann. Phys. (Berlin)* **524**, 479 (2012).
- [5] F. Alemanno *et al.* (DAMPE Collaboration), Search for gamma-ray spectral lines with the dark matter particle explorer, *Sci. Bull.* **67**, 679 (2022).
- [6] H. An, S. Ge, W.-Q. Guo, X. Huang, J. Liu, and Z. Lu, Direct detection of dark photon dark matter using radio telescopes, *Phys. Rev. Lett.* **130**, 181001 (2023).
- [7] J. W. Foster, S. J. Witte, M. Lawson, T. Linden, V. Gajjar, C. Weniger, and B. R. Safdi, Extraterrestrial axion search with the breakthrough listen Galactic center survey, *Phys. Rev. Lett.* **129**, 251102 (2022).
- [8] J. Aalbers *et al.* (LZ Collaboration), First dark matter search results from the LUX-ZEPLIN (LZ) experiment, *Phys. Rev. Lett.* **131**, 041002 (2023).
- [9] E. Aprile *et al.* (XENON Collaboration), First dark matter search with nuclear recoils from the XENONnT experiment, *Phys. Rev. Lett.* **131**, 041003 (2023).
- [10] D. Carney *et al.*, Snowmass2021 cosmic frontier white paper: Ultraheavy particle dark matter, *SciPost Phys. Core* **6**, 075 (2023).
- [11] K. Harigaya, M. Ibe, K. Kaneta, W. Nakano, and M. Suzuki, Thermal relic dark matter beyond the unitarity limit, *J. High Energy Phys.* **08** (2016) 151.
- [12] M. Geller, S. Iwamoto, G. Lee, Y. Shadmi, and O. Telem, Dark quarkonium formation in the early universe, *J. High Energy Phys.* **06** (2018) 135.
- [13] V. K. Dubrovich, D. Fargion, and M. Yu. Khlopov, Primordial bound systems of superheavy particles as the source of ultra-high energy cosmic rays, *Astropart. Phys.* **22**, 183 (2004).
- [14] D. Tak, M. Baumgart, N. L. Rodd, and E. Pueschel, Current and future gamma-ray searches for dark matter annihilation beyond the unitarity limit, *Astrophys. J. Lett.* **938**, L4 (2022).
- [15] L. E. Strigari, Galactic searches for dark matter, *Phys. Rep.* **531**, 1 (2013).
- [16] J. Conrad, and O. Reimer, Indirect dark matter searches in gamma and cosmic rays, *Nat. Phys.* **13**, 224 (2017).
- [17] M. Ackermann *et al.* (Fermi-LAT Collaboration), Constraining dark matter models from a combined analysis of Milky Way satellites with the Fermi Large Area Telescope, *Phys. Rev. Lett.* **107**, 241302 (2011).
- [18] M. Ackermann *et al.* (The Fermi-LAT Collaboration), Searching for dark matter annihilation from Milky Way dwarf spheroidal galaxies with six years of Fermi Large Area Telescope data, *Phys. Rev. Lett.* **115**, 231301 (2015).
- [19] A. Albert *et al.*, Dark matter limits from dwarf spheroidal galaxies with the HAWC gamma-ray observatory, *Astrophys. J.* **853**, 154 (2018).
- [20] A. Albert *et al.*, Search for gamma-ray spectral lines from dark matter annihilation in dwarf galaxies with the High-Altitude Water Cherenkov observatory, *Phys. Rev. D* **101**, 103001 (2020).
- [21] H. Abdallah *et al.* (H.E.S.S. Collaboration), Search for dark matter signals towards a selection of recently detected DES dwarf galaxy satellites of the Milky Way with H.E.S.S., *Phys. Rev. D* **102**, 062001 (2020).
- [22] V. Acciari *et al.*, Combined searches for dark matter in dwarf spheroidal galaxies observed with the magic telescopes, including new data from Coma Berenices and Draco, *Phys. Dark Universe* **35**, 100912 (2022).
- [23] A. Acharyya *et al.*, Search for ultraheavy dark matter from observations of dwarf spheroidal galaxies with VERITAS, *Astrophys. J.* **945**, 101 (2023).
- [24] W.-Q. Guo, Y. Li, X. Huang, Y.-Z. Ma, G. Beck, Y. Chandola, and F. Huang, Constraints on dark matter annihilation from the FAST observation of the Coma Berenices dwarf galaxy, *Phys. Rev. D* **107**, 103011 (2023).
- [25] D. Song, N. Hiroshima, and K. Murase, Search for heavy dark matter from dwarf spheroidal galaxies: leveraging cascades and subhalo models, *J. Cosmol. Astropart. Phys.* **05** (2024) 087.
- [26] T. N. Maity, A. K. Saha, A. Dubey, and R. Laha, Search for dark matter using sub-PeV γ -rays observed by Tibet AS $_{\gamma}$, *Phys. Rev. D* **105**, L041301 (2021).
- [27] M. Ackermann *et al.* (Fermi-LAT Collaboration), Search for dark matter satellites using the FERMI-LAT, *Astrophys. J.* **747**, 121 (2012).
- [28] M. Di Mauro, M. Stref, and F. Calore, Investigating the effect of Milky Way dwarf spheroidal galaxies extension on dark matter searches with Fermi-LAT data, *Phys. Rev. D* **106**, 123032 (2022).
- [29] X.-H. Ma *et al.*, Chapter 1 LHAASO instruments and detector technology, *Chin. Phys. C* **46**, 030001 (2022).
- [30] Z. Cao *et al.*, Ultrahigh-energy photons up to 1.4 petaelectronvolts from 12 gamma-ray galactic sources, *Nature (London)* **594**, 33 (2021).
- [31] Z. Cao *et al.* (LHAASO Collaboration), Exploring Lorentz invariance violation from ultrahigh-energy γ rays observed by LHAASO, *Phys. Rev. Lett.* **128**, 051102 (2022).
- [32] Z. Cao *et al.* (LHAASO Collaboration), Constraints on heavy decaying dark matter from 570 days of LHAASO observations, *Phys. Rev. Lett.* **129**, 261103 (2022).
- [33] F. Aharonian *et al.* (LHAASO Collaboration), Extended very-high-energy gamma-ray emission surrounding PSR J0622 + 3749 observed by LHAASO-KM2A, *Phys. Rev. Lett.* **126**, 241103 (2021).
- [34] Z. Cao *et al.*, A tera-electron volt afterglow from a narrow jet in an extremely bright gamma-ray burst, *Science* **380**, 1390 (2023).

- [35] C. Zhen *et al.*, Introduction to Large High Altitude Air Shower Observatory (LHAASO), *Chin. Astron. Astrophys.* **43**, 457 (2019).
- [36] F. Aharonian *et al.*, Performance of LHAASO-WCDA and observation of the Crab Nebula as a standard candle, *Chin. Phys. C* **45**, 085002 (2021).
- [37] F. Aharonian *et al.*, Observation of the Crab Nebula with LHAASO-KM2A—A performance study, *Chin. Phys. C* **45**, 025002 (2021).
- [38] C. W. Bauer, N. L. Rodd, and B. R. Webber, Dark matter spectra from the electroweak to the Planck scale, *J. High Energy Phys.* **06** (2021) 121.
- [39] A. Esmaili, and P. D. Serpico, Gamma-ray bounds from EAS detectors and heavy decaying dark matter constraints, *J. Cosmol. Astropart. Phys.* **10** (2015) 014.
- [40] J. F. Navarro, C. S. Frenk, and S. D. M. White, A universal density profile from hierarchical clustering, *Astrophys. J.* **490**, 493 (1997).
- [41] See Supplemental Material at <http://link.aps.org/supplemental/10.1103/PhysRevLett.133.061001> for additional details and results, which includes Refs. [39–42].
- [42] Z. Cao *et al.* (LHAASO Collaboration), Measurement of ultra-high-energy diffuse gamma-ray emission of the Galactic plane from 10 TeV to 1 PeV with LHAASO-KM2A, *Phys. Rev. Lett.* **131**, 151001 (2023).
- [43] X. Huang and K. Duan, A 3D likelihood analysis tool for LHAASO-KM2A data, *Proc. Sci. ICRC2021* (2021) 769.
- [44] T. P. Li and Y. Q. Ma, Analysis methods for results in gamma-ray astronomy, *Astrophys. J.* **272**, 317 (1983).
- [45] D. E. Alexandreas *et al.*, Point source search techniques in ultrahigh-energy gamma-ray astronomy, *Nucl. Instrum. Methods Phys. Res., Sect. A* **328**, 570 (1993).
- [46] A. Geringer-Sameth, S. M. Koushiappas, and M. Walker, Dwarf galaxy annihilation and decay emission profiles for dark matter experiments, *Astrophys. J.* **801**, 74 (2015).
- [47] V. Bonnivard *et al.*, Dark matter annihilation and decay in dwarf spheroidal galaxies: The classical and ultrafaint dSphs, *Mon. Not. R. Astron. Soc.* **453**, 849 (2015).
- [48] A. B. Pace *et al.*, Scaling relations for dark matter annihilation and decay profiles in dwarf spheroidal galaxies, *Mon. Not. R. Astron. Soc.* **482**, 3480 (2018).
- [49] R. Fleyscher, L. Fleyscher, P. Nemethy, A. I. Mincer, and T. J. Haines, Tests of statistical significance and background estimation in gamma-ray air shower experiments, *Astrophys. J.* **603**, 355 (2004).
- [50] S. P. Wakely and D. Horan, TeVCat: An online catalog for very high energy gamma-ray astronomy, in *Proceedings of the 30th International Cosmic Ray Conference* (2007), Vol. 3, pp. 1341–1344.
- [51] Z. Cao *et al.* (LHAASO Collaboration), The first LHAASO catalog of gamma-ray sources, *Astrophys. J. Suppl. Ser.* **271**, 25 (2024).
- [52] G. Cowan, K. Cranmer, E. Gross, and O. Vitells, Asymptotic formulae for likelihood-based tests of new physics, *Eur. Phys. J. C* **71**, 1554 (2011).
- [53] X.-K. Guo, Y.-F. Lü, Y.-B. Huang, R.-L. Li, B.-Y. Zhu, and Y.-F. Liang, Searching for dark-matter induced neutrino signals in dwarf spheroidal galaxies using 10 years of IceCube public data, *Phys. Rev. D* **108**, 043001 (2023).
- [54] G. Steigman, B. Dasgupta, and J. F. Beacom, Precise relic WIMP abundance and its impact on searches for dark matter annihilation, *Phys. Rev. D* **86**, 023506 (2012).
- [55] M. Ackermann *et al.*, Constraints on the galactic halo dark matter from Fermi-LAT diffuse measurements, *Astrophys. J.* **761**, 91 (2012).
- [56] V. Acciari *et al.*, Constraining dark matter lifetime with a deep gamma-ray survey of the Perseus galaxy cluster with magic, *Phys. Dark Universe* **22**, 38 (2018).
- [57] M. G. Aartsen *et al.*, Search for neutrinos from decaying dark matter with IceCube, *Eur. Phys. J. C* **78**, 831 (2018).
- [58] A. Albert *et al.* (HAWC Collaboration), Search for decaying dark matter in the Virgo cluster of galaxies with HAWC, *Phys. Rev. D* **109**, 043034 (2024).
- [59] V. Bonnivard, C. Combet, D. Maurin, and M. G. Walker, Spherical Jeans analysis for dark matter indirect detection in dwarf spheroidal galaxies—Impact of physical parameters and triaxiality, *Mon. Not. R. Astron. Soc.* **446**, 3002 (2015).
- [60] V. Bonnivard, D. Maurin, and M. G. Walker, Contamination of stellar-kinematic samples and uncertainty about dark matter annihilation profiles in ultrafaint dwarf galaxies: The example of Segue I, *Mon. Not. R. Astron. Soc.* **462**, 223 (2016).
- [61] N. Klop, F. Zandanel, K. Hayashi, and S. Ando, Impact of axisymmetric mass models for dwarf spheroidal galaxies on indirect dark matter searches, *Phys. Rev. D* **95**, 123012 (2017).
- [62] J. L. Sanders, N. W. Evans, A. Geringer-Sameth, and W. Dehnen, Indirect dark matter detection for flattened dwarf galaxies, *Phys. Rev. D* **94**, 063521 (2016).
- [63] K. Ichikawa, M. N. Ishigaki, S. Matsumoto, M. Ibe, H. Sugai, K. Hayashi, and S.-i. Horigome, Foreground effect on the J -factor estimation of classical dwarf spheroidal galaxies, *Mon. Not. R. Astron. Soc.* **468**, 2884 (2017).
- [64] P. Ullio and M. Valli, A critical reassessment of particle dark matter limits from dwarf satellites, *J. Cosmol. Astropart. Phys.* **07** (2016) 025.
- [65] K. Hayashi, K. Ichikawa, S. Matsumoto, M. Ibe, M. N. Ishigaki, and H. Sugai, Dark matter annihilation and decay from non-spherical dark halos in galactic dwarf satellites, *Mon. Not. R. Astron. Soc.* **461**, 2914 (2016).